https://doi.org/10.1016/j.camwa.2016.07.005

LBM Simulation on the Influence of Endothelial SGL Structure on Cell Adhesion in the Micro-vessels

Weiwei Yan[1], Yang Liu[2*] and Bingmei Fu[3]

[1]College of Metrology and Measurement Engineering, China Jiliang University, Hangzhou, China

[2]Department of Mechanical Engineering, The Hong Kong Polytechnic University, Kowloon, Hong Kong

[3]Department of Biomedical Engineering, The City College of the City University of New York, New York, USA

Abstract

The endothelial surface glycocalyx layer (SGL) plays a crucial role in modulating vascular permeability, sensing hydrodynamic changes and attenuating cell adhesion in microcirculation. In this work, the effect of endothelial SGL structure on cell adhesion was numerically studied in the uneven micro-vessel caused by the shedding of endothelial SGL. The blood dynamics was conducted by the LBM, the adhesive dynamics was performed by the stochastic Monte Carlo method, and the cell dynamics was executed by the Newton's law. To validate the numerical schemes, the cell suspension flow in the symmetric stenotic vessel and the leukocyte adhesion in the straight vessel were executed firstly. The simulation results show that the present numerical schemes are capable of studying cell suspension behavior and leukocyte adhesive phenomenon in the 2-D vessels, and the leukocyte adhesive states, including no adhesion, rolling, landing and firm adhesion, can be successfully recreated. Furthermore, it is found that the endothelial SGL structure significantly influences cell adhesion function, by changing the geometry of the micro-vessel, providing more ligands to form receptor-ligand bonds, and enhancing the forward reaction rate for the forming of new bonds. The present results may be helpful in understanding the mechanical mechanism of the cell adhesion function with the shedding of the endothelial SGL in microcirculation.

Keywords: lattice Boltzmann method, cell adhesion, endothelial SGL, adhesive dynamics model

1. INTRODUCTION

The endothelial SGL plays a crucial role in modulating vascular permeability, sensing hydrodynamic changes and attenuating cell adhesion in microcirculation. Loss of endothelial SGL has been found in many vascular diseases, such as diabetes, inflammation, ischemia, atherosclerosis and tumor metastasis, to name a few. Much of the previous literature on endothelial SGL has been summarized in several excellent reviews (Weinbaum et al. 2007; Tarbell 2010; Fu and Tarbell 2013).

The structure of endothelial SGL has been widely studied since the 1960s, owing to its critical role in regulating vascular functions. The first visualization of endothelial SGL was carried out by transmission electron microscopy with the use of probe ruthenium red, which allowed the estimation of the thickness of SGL to be ~0.02 μm in capillaries (Luft 1966). The first indirect in vivo measurement of SGL thickness was executed by using intravital microscopy (Vink and Duling1996). It was found that the SGL thickness in hamster cremaster muscle capillaries is about 0.4-0.5 μm, which is nearly 15-20% of the radius of the smallest capillary. The direct measurement of SGL thickness has been performed via several techniques, such as laser scanning confocal microscopy, fluorescence microscopy, and multi-photon microscopy, which revealed a much thicker SGL in the large blood vessels (Reitsma et al. 2011). Recently, Yen et al. (2012) quantified the thickness of SGL on the micro-vessels of rat mesentery and mouse cremaster muscle in situ based on in vivo immunolabeling and laser scanning confocal microscopy. The results suggested that about 1 μm thick SGL is covered on the capillaries, and nearly 2 μm thick SGL is spread over the aortas, and the SGL is discontinuously and unevenly distributed along the inner surface of the micro-vessels.

As a barrier between circulating cells and the microvessel wall, the endothelial SGL plays an important role in cell adhesion in microcirculation. Based on the experimental observations, Sabri et al. (2000) demonstrated that the living cells actually apply SGL modulation to mediate adhesiveness, and this modulation is a physiological means of regulating cell adhesion. Mulivor and Lipowsky (2002) experimentally investigated the role of glycocalyx in the leukocyte-endothelial cell adhesion. They indicated that the SGL serves as a barrier to cell adhesion, and its shedding during natural activation of endothelial cells (ECs) may be an essential part of the inflammatory response. Subsequent work by Lipowsky (2012) further

revealed the shedding of SGL exposes adhesion ligands and therefore enhances cell adhesion. Most of the previous studies on the effect of SGL on cell adhesion were conducted by the experimental methods.

With the improvement of biomechanical measurement technology, various mathematical models have been proposed to study cell adhesion under hydrodynamic conditions, which eventually propels the development of adhesive dynamics models. Hammer and Apte (1992) proposed the first adhesive dynamics model that can simulate the effect of many parameters on cell adhesion, such as the number of receptors, the density of ligand, the reaction rates for adhesive bonds, and the response of springs to strain. Since then, numerous modifications and refinements of the models were improved to simulate single leukocyte adhesion, multiple leukocytes adhesion, and tumor cell adhesion. In these models, the receptor-ligand bonds stochastically form and break according to the probabilities that determined by the forward and reverse reaction rates.

Despite significant studies have been performed in cell adhesion, the precise mechanical mechanism of cell-endothelial adhesion in micro-vessels with discontinuously and unevenly distributed SGL is not yet clearly understood, owing to the complexities of blood dynamics, SGL structure, and cell-surface adhesive interactions involved. The objective of this work is to numerically study the effect of endothelial SGL structure on cell adhesion in the micro-vessels. In the simulations, the blood dynamics is carried out by the lattice Boltzmann method (LBM) (Chen and Doolen 1998), the adhesive dynamics is solved by the stochastic Monte Carlo method, and the cell dynamics is governed by the Newton's law with translation and rotation.

2. METHODS

2.1 Problem Description

Since the endothelial SGL is intermittently and unevenly covered the inner surface of blood vessels (Yen et al. 2012), the 2-D micro-vessel with three regions of SGL deficiency, which are composed of a large negative curved vessel with a radius of curvature of 55 μm and a small positive curved vessel with a radius of curvature of 2.25 μm, is illustrated in Fig. 1. Besides, all the straight parts of the micro-vessels are assumed to be covered with continuous and adequate SGL. The total length and the height of the micro-vessel is L = 500 μm and H =

40 μm, respectively. The length of three curved vessels is L_3 = 30 μm, and the length of two straight segments is L_4 = 30 μm. The height of the SGL deficiency regions is h = 2 μm, which is analogous to the SGL thickness of the experimental data (Yen et al. 2012). To avoid the effect of entrance on cell adhesion, the entrance length is set as L_2 = 175 μm. Here, we use the configuration of leukocyte to represent the circulating cell, and the diameter of the cell is chosen as d = 10 μm, which is the typical size of the leukocyte. The cell is placed in the straight part of the micro-vessel at (135μm, 7.03μm), and driven by a pressure difference Δp = 10 Pa that set between the left inlet and right outlet. The red region is the total computational domain.

2.2 LBM for Blood Dynamics

The LBM has been a promising numerical tool to effectively model complex physics in CFD, which has simple formulations, efficient parallel computing, and easy treatment of complex boundary conditions. In this study, the LBM is adopted to implement the blood dynamics (see Fig. 2a). The lattice Boltzmann equation with the BGK collision operator is expressed as,

$$f_i(\vec{x}+\vec{e}_i\delta x, t+\delta t) - f_i(\vec{x},t) = -\frac{1}{\tau}\left[f_i(\vec{x},t) - f_i^{eq}(\vec{x},t)\right] \tag{1}$$

where $f_i(\vec{x},t)$ is the distribution function (DF) for the particle with velocity $\vec{e}_i$ at position $\vec{x}$ and time t, δt is the time increment, δx is the length of lattice, $c = \delta x/\delta t$ is defined as the lattice speed, τ is the relaxation time, and $f_i^{eq}(\vec{x},t)$ is the equilibrium DF. Based on the D_2Q_9 model, the equilibrium DF can be chosen as,

$$f_i^{eq}(\vec{x},t) = \rho w_i\left[1+\frac{3}{c^2}(\vec{e}_i\cdot\vec{u})+\frac{9}{2c^4}(\vec{e}_i\cdot\vec{u})^2-\frac{3}{2c^2}\vec{u}^2\right] \tag{2}$$

where w_i is the weight coefficients given by $w_0 = 4/9$, $w_i = 1/9$ for $i = 1-4$, and $w_i = 1/36$ for $i = 5-8$. Finally, the blood density ρ and momentum $\rho\vec{u}$ are calculated by,

$$\rho = \sum f_i(\vec{x},t) = \sum f_i^{eq}(\vec{x},t) \tag{3}$$

$$\rho \vec{u} = \sum \vec{e}_i f_i(\vec{x},t) = \sum \vec{e}_i f_i^{eq}(\vec{x},t) \tag{4}$$

2.3 Stochastic Monte Carlo Method for Adhesive Dynamics

The adhesive dynamics is solved by the stochastic Monte Carlo method. As shown in Fig. 2b, the cell is idealized as a disk. The adhesion molecules on the tips of microvillus covered on the cell are modeled as the receptors, and the substrate is composed of ECs that provide a high density of ligands. Once the distances between ligands and receptors are smaller than the critical length H_c, they have the chance to form ligand-receptor bonds, which are idealized as adhesive springs. The stochastic kinetic rate expressions relate the forward formation reaction rate k_f (Dembo *et al.* 1988) and the reverse dissociation reaction rate k_r (Bell 1978), they are,

$$k_f = k_f^0 \exp\left(-\frac{\sigma_{ts}(\chi-\lambda)^2}{2k_bT}\right) \tag{5}$$

$$k_r = k_r^0 \exp\left(\frac{\gamma f}{k_bT}\right) \tag{6}$$

where k_b is the Boltzmann constant, T is the temperature, χ is the bond length, λ is the equilibrium bond length, k_f^0 and k_r^0 are the reaction rate constants at their equilibrium states, σ_{ts} is the transition state spring constant, γ is the microvillus reactive compliance, and $f = \sigma(\chi-\lambda)$ is the spring force of each bond calculated according to the Hooke's law. The appropriate expressions for the probability of bond forming and breaking tethers in a time step dt are (Chang and Hammer 1996),

$$P_f = 1-\exp(-k_f dt) \tag{7}$$

$$P_r = 1-\exp(-k_r dt) \tag{8}$$

where P_f is the probability of forming bonds, and P_r is the probability of breaking bonds in a

time interval *dt*. Based on the stochastic Monte Carlo method, the adhesive spring force $\vec{F}_s$ is computed by the summation of all the compressed or expanded springs,

$$\vec{F}_s = \sum_{i=1}^{n} \sigma(\chi_i - \lambda) \tag{9}$$

where *n* is the total number of the receptor-ligand bonds.

The implement of stochastic Monte Carlo method for adhesive dynamics follows two steps. In the bond formation step, the distances between receptors and ligands are calculated via $d_{rl} = \left[(x_r - x_l)^2 + (y_r - y_l)^2 \right]^{0.5}$, where ($x_r$, y_r) and (x_l, y_l) are the locations of receptors and ligands. Then, the distances d_{rl} are compared to the critical length H_c. If $d_{rl} \geq H_c$, the receptors and ligands have no chance to form new bonds. However, if $d_{rl} < H_c$, the receptors and ligands have chance to form receptor-ligand bonds. Concretely, the formation probability $P_f \in (0, 1)$ is computed via Eqn. (7), and the computer also generates a stochastic number $N_f \in (0, 1)$. If $P_f \geq N_f$, the receptors and ligands are bounded to form new bonds; otherwise, the receptors and ligands still keep free. In the bond breakage step, a preexisting bond may be broken with probability $P_r \in (0, 1)$ calculated according to Eqn. (8). Likewise, the breakage probability P_r is compared to another random number $N_r \in (0, 1)$. If $P_r \geq N_r$, the bond is broken up into free receptor and ligand; otherwise, the bond is still bounded.

2.4 Newton's Law for Cell Dynamics

The cell dynamics (see Fig. 2c) follows the Newton's law of translation and rotation, namely,

$$m\frac{d\vec{u}}{dt} = \vec{F};\ I\frac{d\omega}{dt} = T \tag{10}$$

where $\vec{u}$ is the velocity of cell, ω is the angular velocity, T is the torque, I is the inertia, m is the mass, and $\vec{F} = \vec{F}_s + \vec{F}_h + \vec{F}_v$ is the total force that acting on the cell, where $\vec{F}_s$ is the spring forces computed by Eq. (9), $\vec{F}_h$ is the hydrodynamic force calculated based on the momentum exchange method (Ladd 1994), and $\vec{F}_v$ is the repulsive van der Waals force which can be obtained by (Bongrand and Bell 1984),

$$\vec{F}_v = \frac{A}{8\sqrt{2}}\sqrt{\frac{R}{\varepsilon^5}} \quad (11)$$

where R is the radius of the cell, ε is the separation distance between the surfaces of cell and ECs, $A = 5\times10^{-20}$ J is the repulsive Hamaker constant. At each time step, the position and angle of the cell are determined by,

$$\vec{u} = \frac{d\vec{x}}{dt};\ \omega = \frac{d\theta}{dt} \quad (12)$$

where θ is the rotational angle of the cell. For the purpose of stability, the leap-frog algorithm was applied to update the velocity, position, angular velocity and angle of the cell with the increment of time.

Totally, the computational steps in executing cell adhesion and migration at each time step are briefly summarized as follows. Step 1: Calculate the external forces, i.e. $\vec{F}_h$, $\vec{F}_s$, $\vec{F}_v$, acting on the cell. Step 2: Check for the formation and breakage of the receptor-ligand bonds based on Eqs. (5-8). Step 3: Update the position and angle of the cell under flow condition based on Eqs. (10) and (12). Step 4: Update the lengths of the bound microvilli. With the end of step 4, the time is updated and the process is repeated until the end of the simulations.

3. RESULTS AND DISCUSSION

3.1 Method Validation

3.1.1 Cell suspension in the symmetric stenotic vessel

To evaluate the accuracy and reliability of present numerical method, the cell suspension flow is firstly performed in a 2-D symmetric stenotic vessel. This kind of cell suspension flow through stenosis vessels is of great interest in medical science (Li et al. 2004). As shown in Fig. 3(a), the geometry of stenotic vessel is designed as a 2-D planar vessel with the length L = 32d and the height H = 8d. Here, d = 8.5 μm is the diameter of the cell. The stenosis is established by adding two symmetric protuberances inside the vessel. The protuberance is a semicircle with the radius determined by the width of stenosis throat b, where b = 1.75d. The cell is initially placed in the left of stenosis throat at (8d, 6d), and it moves through the stenosis

throat towards the outlet driven by a pressure drop Δp = 541 Pa. The simulation parameters and their values adopted are listed in Table 1. The calculation is performed using 544×136 lattice grid, which is sufficient to provide numerical convergence. One time step corresponds to a physical time of 1.74×10^{-8} s.

The snapshots of position and rotation angle of the cell against the time and x-axis are shown in Fig. 3(a). The cell moves towards the centerline when it gets near and across the protuberance, but it never arrives at the centerline of the vessel. Once passing through the stenosis, the cell migrates up to the same height of the initial position, of which 2d above the centerline. This result is consistent with the Segré-Silberberg effect observed in the flat pipe flow, of which neutrally buoyant cylinders migrated laterally away from both the wall and the centerline and reached a certain lateral equilibrium position (Segré and Silberberg 1961). The flow vectors are plotted and illustrated in Fig. 3(b). The cell moves and rotates, and passes through the stenosis under flow condition. The flow vectors in the stenosis are much larger and denser than those in the straight part of the vessel.

Fig. 3 (c) displays x, y-component velocities and angular velocity of the cell against x-axis value. The x-component velocity at the stenosis throat reaches a peak, with which the amplitude is about 5 times of that in the straight part of the vessel. The y-component velocity changes its direction at the stenosis throat, and two peaks appear at x = 119 μm and 153 μm. The trend of angular velocity is similar to that of x-component velocity. It indicates that the cell rotates more quickly at the stenosis throat than that in the flat vessel. All the current simulation results match those reported by Wu and Shu (2010). Moreover, the simulation results are quantitatively compared with those of Li et al. (2004). From Fig. 3(c), it is found that the simulation results agree well with each other, which verify that our numerical method is capable of studying cell suspension and migration behavior in the 2-D blood vessels.

3.1.2 Leukocyte adhesion in the straight micro-vessel

To further validate the reliability of present numerical method that coupled the stochastic adhesive dynamics, the single leukocyte adhesion in a straight micro-vessel is numerically examined. The leukocyte adhesion to ECs plays a crucial role in the inflammatory response. The process has been intensively studied and referred to as leukocyte adhesion cascade. To successfully recreate the leukocyte adhesive states, including capture, rolling, landing, and

firm adhesion, the leukocyte adhesion with different values of the Bell's model parameters is executed. The length and the height of the vessel is L = 420 μm and H = 40 μm, respectively. The diameter of the leukocyte is set as d = 10 μm, the pressure drop is set as Δp = 10 Pa, and the values of other simulation parameters are listed in Table 1. The simulations are executed using 1680×160 lattice grid, and the time step corresponds to a physical time of 4.35×10^{-9} s.

By setting the Bell's model parameters with $\gamma = 0.5$ Å and $k_r^0 = 200\ \mathrm{s}^{-1}$, the trace of the leukocyte in the rolling state is shown in Fig. 4(a). It is seen that the leukocyte travels steadily along the vessel wall with translation and rotation. Fig. 4(b) shows the simultaneous number of bonds for a representative rolling leukocyte. After a short traveling, the total number of bonds of the leukocyte fluctuates from 1 to 15 with an average of about 9, never falling below one bond, thus the leukocyte is always bound to the surface of ECs. The stretched bonds, which provide a large component of spring forces to act in a direction to overcome the hydrodynamic shear force from the surrounding blood, can also reduce the instantaneous velocity and angular velocity of the leukocyte due to the adhesion effect.

To further study the leukocyte adhesive states, we modeled a series of cases of leukocyte adhesion in the straight micro-vessel with different reactive compliances γ and unstressed dissociation rates k_r^0. In the simulations, we set γ and k_r^0 as: A. 0.5 Å and 1000 s^{-1}; B. 0.5 Å and 200 s^{-1}; C. 0.75 Å and 20 s^{-1}; and D. 0.5 Å and 20 s^{-1}. The other simulation parameters and their values are tabulated in Table 1. The representative trace of adhesion behavior states are displayed in Fig. 4(c). Case A corresponds to no adhesion state, case B stands for the rolling state, case C represents the landing state, and case D corresponds to the firm adhesion state. It is statistically calculated that the average velocities of the leukocytes for no adhesion, rolling and firm adhesion states are approximately 40%V_h, 6.5%V_h and 0.9%V_h, respectively. Here, V_h is the hydrodynamic free-stream velocity. For the landing case, the leukocyte firstly circulates with a high velocity and then suddenly firmly adheres to the endothelial wall at about t = 0.3 s. Moreover, one can find that the reactive compliances γ and the unstressed dissociation rate k_r^0 have greatly effects on leukocyte adhesion. The larger unstressed dissociation rate results in stronger leukocyte adhesion, and the smaller reactive compliance causes firmer leukocyte adhesion. The observations of our numerical simulations agree well with the definition of adhesion behavior states in King and Hammer (2001) and Caputo and Hammer (2005), which

reveals that the present numerical method is capable of modeling various cell adhesion states.

3.2 Effect of Endothelial SGL Structure on Cell Adhesion in the Micro-vessel

It was recognized that cell adhesion is related to the properties of receptor and ligand, such as modulation of surface receptor and ligand density, topographical distribution of receptor and ligand on cell membranes, and affinity of kinetic parameters for receptor-ligand reactions (Chang et al. 2000, Yan et al. 2012). In this study, the effects of the geometry of vessel, density of ligand, and forward reaction rate of ligand, all of which are resulted from the shedding of endothelial SGL, on cell adhesion are quantitatively investigated by the LBM which simultaneously couples the stochastic Monte Carlo method to model adhesive dynamics. First of all, as a referential case, the cell adhesion in the uneven micro-vessel with uniform density of ligands is numerically executed. Here, the normal density of ligand is N_L = 47/μm^2, which means 600 ligands distributed around the cylinder circumference spaced every 0.45μm (Chang and Hammer 1996). The reactive compliance and unstressed dissociation rate are chosen as $\gamma = 1$ Å and $k_r^0 = 200\ \mathrm{s}^{-1}$, respectively. The other simulation parameters and their values adopted have been tabulated in Table 1.

Fig 5(a) shows the trace of the cell with translation and rotation along the uneven micro-vessel. It can be found that the traces in the curved segments are slightly denser than these in the straight parts, and the angular velocities of the cell in the curved segments are also smaller than those in the straight segments, both of which are contributed to the stronger cell adhesion effect in the curved segments. The *x*, *y*-component velocities of the cell is illustrated in Fig. 5(b). It can be clearly seen that the geometry of the vessel could influence cell adhesion. The *x*-component velocities in three curved segments are much smaller, with which the average value is about 300μm/s, much smaller than 800μm/s in the straight sections. The *y*-component velocity in the straight segments is almost flat, but it experiences valleys and peaks in the curved parts and change direction in the middle of the sunken region. The effect of cell adhesion can further be reflected by the number of bonds, which is shown in Fig. 5(c). One can find that the number of bonds fluctuates between 0 and 6 due to stochastic cell adhesion effect, and the largest number of bonds of 6 takes place in the first and second sunken regions. Overall, the influence of the geometry of vessel on cell adhesion is comparatively weak.

The shedding of endothelial SGL would expose more adhesion ligands and thus enhance cell adhesion function. In this study, the density of ligand in SGL deficiency regions is assumed to be 10 times of the normal case, namely, N_L = 470/μm^2, while the density of ligand in the straight segments is still keep to be N_L = 47/μm^2. The effect of the heterogeneous density of ligand on cell adhesion is carried out on the uneven micro-vessel. The values of other simulation parameters are set as the same as the referential case.

The trace of the cell in the uneven vessel with heterogeneous densities of ligand is shown in Fig. 6(a). Different from the referential case, the traces in the first and second SGL deficiency regions are rather dense, and the angular velocity of the cell is also much smaller in these two regions due to stronger cell adhesion there. The cell finally stops in the second SGL deficiency region, which means that it firmly adheres to the vessel wall. The heterogeneous densities of ligand also result in the variation of *x*, *y*-component velocities during cell moving, which is illustrated in Fig. 6(b). Similar to the referential case, the maximum amplitude of *x*-component velocity in the straight sections is about 900μm/s. However, the *x*-component velocity in the first SGL deficiency region nearly approaches to zero, and both of *x*, *y*-component velocities arrive at zero in the middle of the second SGL deficiency region, where firm adhesion take places. The simultaneous number of bonds in the whole process is shown in Fig. 6(c). It is seen that the number of bonds fluctuates between 0 and 5 in the straight segments, which is in common with that of the referential case. Nevertheless, the number of bonds sharply increases and fluctuates between 11 and 31 in two collapsed regions. From Fig. 6, it is found that the endothelial SGL structure greatly affects cell adhesion function by providing more ligands to form adhesive bonds.

The cell adhesion is related to the affinity of kinetic parameters for receptors and ligands reactions. We assume that the shedding of endothelial SGL would increase forward reaction rate and hence strengthen cell adhesion. Here, the intrinsic forward reaction rate in the sufficient SGL region is set as the same as the referential case, namely, $k_f^0 = 10^{-2}$ s, while it in the sunken SGL deficiency regions is set to be 10 times of that in the SGL sufficiency regions, namely, $k_f^0 = 10^{-1}$ s. In the next, the effect of the forward reaction rate on cell adhesion in the uneven micro-vessel is numerically investigated. The values of other simulation parameters are set as the same as the referential case.

Fig. 7(a) shows the trace of the cell with non-uniform intrinsic forward reaction rates in the uneven micro-vessel. In this case, the density of trace is extraordinary dense in the first cupped region, where extremely firm cell adhesion occurs. It is found that the cell strongly adheres to the vessel wall in the first SGL deficiency region, where *x*, *y*-component velocities eventually tend to zero, as shown in Fig. 7(b). From Fig. 7(c), one can find that the number of bonds experiences rapidly augment from the straight portion to the first SGL deficiency region. Like the referential case, the number of bonds in the straight section fluctuates between 0 and 5. However, the maximum number of bonds in the first sunken region is 29, almost 4 times of that in the straight segment. The large number of bonds results in the firm adhesion in the SGL deficiency region. Based on Fig. 7, it is suggested that the endothelial SGL structure significantly influences cell adhesion by raising forward reaction rate between receptors and ligands.

4. CONCLUSIONS

In this study, the effect of endothelial SGL structure on cell adhesion was computationally investigated in the uneven micro-vessel that resulted from the shedding of endothelial SGL, which simultaneously causes the variation of the density of ligand and the forward reaction rate of ligand. As the validation cases, the cell suspension flow in the 2-D symmetric stenotic blood vessel and the leukocyte adhesion in the 2-D straight micro-vessel were performed to test the reliability of the numerical schemes. In the simulations, the blood dynamics was conducted by the LBM, the adhesive dynamics was performed by the stochastic Monte Carlo method, and the cell dynamics was executed by the Newton's law. The simulation results lead to the following conclusions:

(1) The present numerical method is capable of studying the cell suspension behavior and leukocyte adhesion effect in the 2-D blood vessels.

(2) The present numerical method can successfully recreate the leukocyte adhesive behavior in the 2-D straight micro-vessel, including no adhesion, rolling, landing and firm adhesion, by adopting the appropriate values of unstressed dissociation rate and reactive compliances.

(3) The endothelial SGL structure significantly influences cell adhesion function, by changing the geometry of the micro-vessel, providing more ligands to form receptor-ligand bonds, and increasing the forward reaction rate for the forming of new bonds, in the uneven micro-vessel.

(4) ACKNOWLEDGEMENT

Supports given by NSF of China 11202203, NSF of Zhejiang LY15A020005, HKRGC PolyU 5202/13E, PolyU G-YL41, and NIH grant SC1CA153325-01 of the USA are gratefully acknowledged.

REFERENCES

Bell G.I. 1978. Models for the specific adhesion of cells to cells. Science. 200: 618-627

Bongrand P. and Bell G.I. 1984. Cell-cell adhesion: parameters and possible mechanisms. Marcel Dekker, NewYork

Caputo K.E. and Hammer D.A. 2005. Effect of microvillus deformability on leukocyte adhesion explored using adhesive dynamics simulations. Biophys. J. 89: 187-200

Chang K.C. and Hammer D.A. 1996. Influence of direction and type of applied force on the detachment of macromolecularly-bound particles from surfaces. Langmuir 12: 2271-2282

Chang K.C., Tees D.F.J. and Hammer D.A. 2000. The state diagram for cell adhesion under flow: leukocyte rolling and firm adhesion. PNAS, 12, 2271-2282

Chen S. and Doolen G.D. 1998. Lattice Boltzmann method for fluid flows. Annu. Rev. Fluid Mech. 30, 329-364

Dembo M., Torney D.C., Saxman K. and Hammer D.A. 1988. The reaction-limited kinetics of membrane-to-surface adhesion and detachment, Proc. R. Soc. Lond. B. Biol. Sci., 234, 55-83.

Fu B.M .and Tarbell J.M. 2013. Mechano-sensing and transduction by endothelial surface glycocalyx: composition, structure and function, in “Endothelial mechanobiology: computational and experimental methods” in Systems Biology in Medicine and Biology, Wiley Interdiscip Rev Syst Biol Med. 5(3):381-90.

Hammer D.A. and Apte S.M. 1992. Simulation of cell rolling and adhesion on surfaces in shear flow: general results and analysis of selectin-mediated neutrophil adhesion. Biophys. J. 63: 35-57

King M.R. and Hammer D.A. 2001. Multiparticle adhesive dynamics: Hydrodynamic recruitment of rolling leukocytes, PNAS, 98, 14919-14924.

Ladd A.C.J. 1994. Numerical simulation of particulate suspensions via a discretized Boltzmann equation. J. Fluid Mech. 271: 285–309

Li H.B., Fang H.P., Lin Z.F., Xu S.X. and Chen Y.Y. 2004. Lattice Boltzmann simulation on particle suspensions in a two-dimensional symmetric stenotic artery. Phys. Rev. E, 69, 031919

Lipowsky H.H. 2012. The endothelial glycocalyx as a barrier to leukocyte adhesion and its mediation by extracellular proteases. Ann. Biomed. Eng. 40 (4): 840-848

Luft J.H. 1966. Fine structures of capillary and endocapillary layer as revealed by ruthenium red. Fed. Proc. 25, 1773-1783.

Mulivor A.W. and Lipowsky H.H. 2002. Role of glycocalyx in leukocyte-endothelial cell adhesion. Am. J. Physiol. Heart Circ. Physiol. 283, H1282-H1291.

Reitsma S., oude Egbrink M.G., Vink H., van den Berg B.M., Passos V.L., Engels W., Slaaf D.W. and van Zandvoort M.A. 2011. Endothelial glycocalyx structure in the intact carotid artery: a two-photon laser scanning microscopy study. J. Vasc. Res. 48, 297-306.

Sabri S., Soler M., Foa C., Pierres A., Benoliel A. and Bongrand P. 2000. Glycocalyx modulation is a physiological means of regulating cell adhesion. J. Cell Sci. 113, 1589-1600.

Segré G. and Silberberg A. 1961. Radial particle displacements in Poiseuille flow of suspensions, Nature, 189, 219

Skalak R. and Chien S. 1987. Handbook of Bioengineering, McGraw-Hill, New York

Tarbell J.M. 2010. Shear stress and the endothelial transport barrier. Cardiovasc. Res. 87, 320-330.

Vink H. and Duling B.R. 1996. Identification of distinct luminal domains for macromolecules, erythrocytes, and leukocytes within mammalian capillaries. Circ Res 79:581-589

Weinbaum S., Tarbell J.M. and Damiano E.R. 2007. The structure and function of the

endothelial glycocalyx layer. Annu. Rev. Biomed. Eng. 9, 121-167.

Wu J. and Shu C. 2010. Particulate flow simulation via a boundary condition-enforced immersed boundary-lattice Boltzmann scheme. Commun. Comput. Phys. 7, 793-812.

Yan W.W., Liu Y. and Fu B.M. 2012. Effects of wall shear stress and its gradient on tumor cell adhesion in curved microvessels. Biomech. Model. Mechanobiol. 11, 641-653.

Yen W.Y., Cai B., Zeng M., Tarbell J.M. and Fu B.M. 2012. Quantification of the endothelial surface glycocalyx on rat and mouse blood vessels. Microvasc. Res. 83 (3): 337-46.

Table 1 Simulation parameters and their values

Parameter	Definition	Value (reference)
H_c	cut-off length for bond formation	40 nm (Chang et al. 2000)
ρ	plasma density	1.05 g/cm^3 (Skalak and Chien 1987)
v	plasma kinetic viscosity	1.2 × 10^{-6} m^2/s (Skalak and Chien 1987)
T	temperature	310 K (Chang and Hammer 1996)
[illegible]	equilibrium bond length	20 nm (Chang and Hammer 1996)
k_b	Boltzmann constant	1.38 × 10^{-23} J/K
N_L	density of ligand	47/μm^2 (Chang and Hammer 1996)
[illegible]	intrinsic forward reaction rate	10^{-2}/s (Dembo et al. 1988)
[illegible]	spring constant	2 × 10^{-3} N/m (Chang and Hammer 1996)
[illegible]	transition state spring constant	10^{-3} N/m (Chang and Hammer 1996)

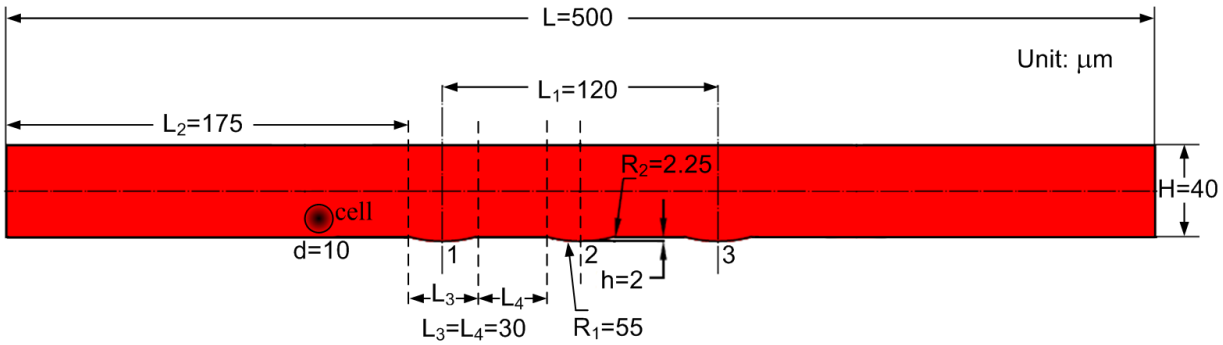

Figure 1. The schematic view of 2-D micro-vessel

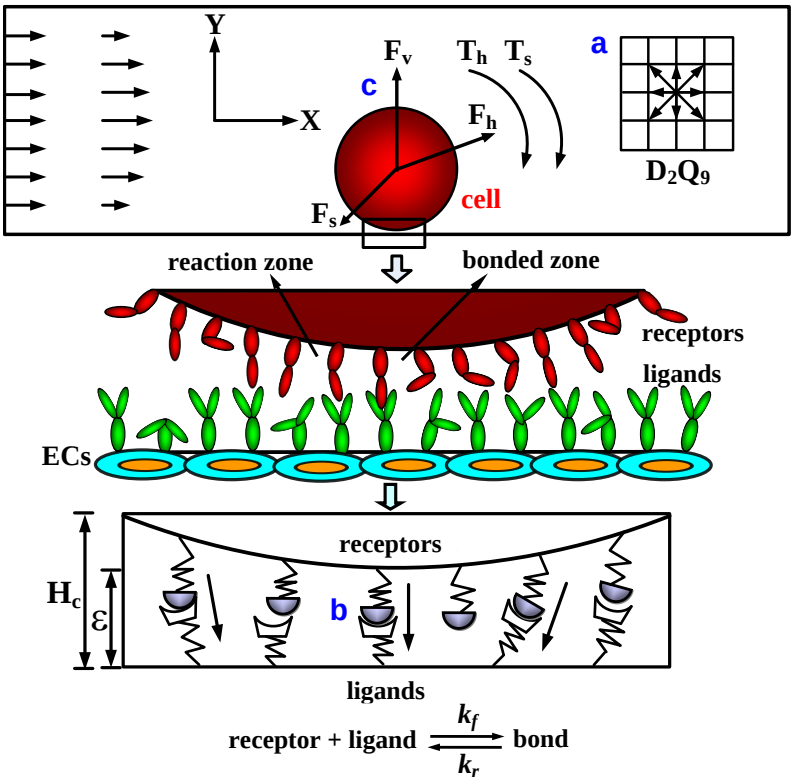

Fig. 2. The schematic view of simulation dynamics: (a) blood dynamics, (b) adhesive dynamics, and (c) cell dynamics.

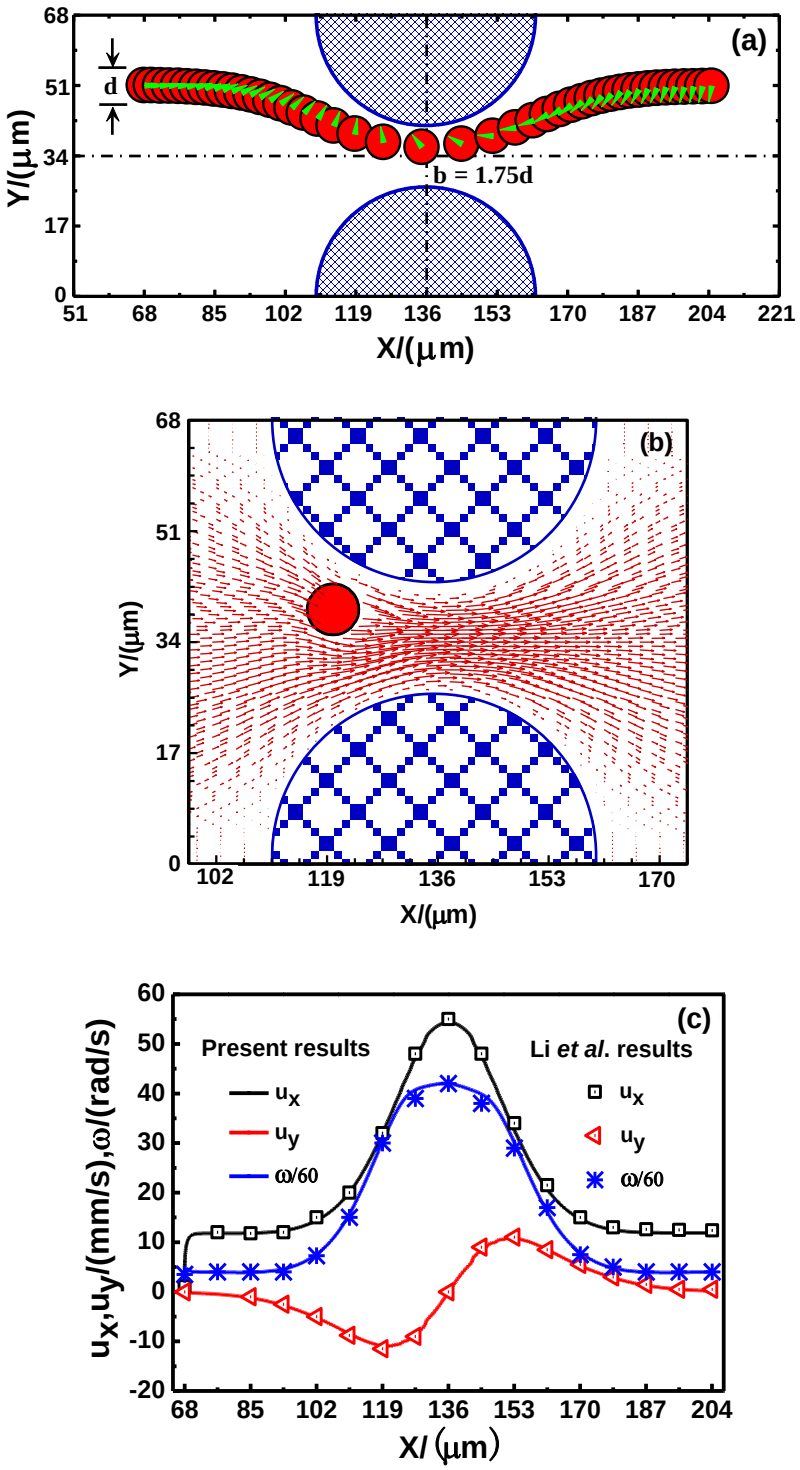

Fig. 3. (a) The geometry of the stenotic vessel and the snapshots of the cell, (b) The flow vectors in the stenotic vessel, and (c) The *x*, *y*-component velocity and angular velocity of the cell against the *x*-axis value.

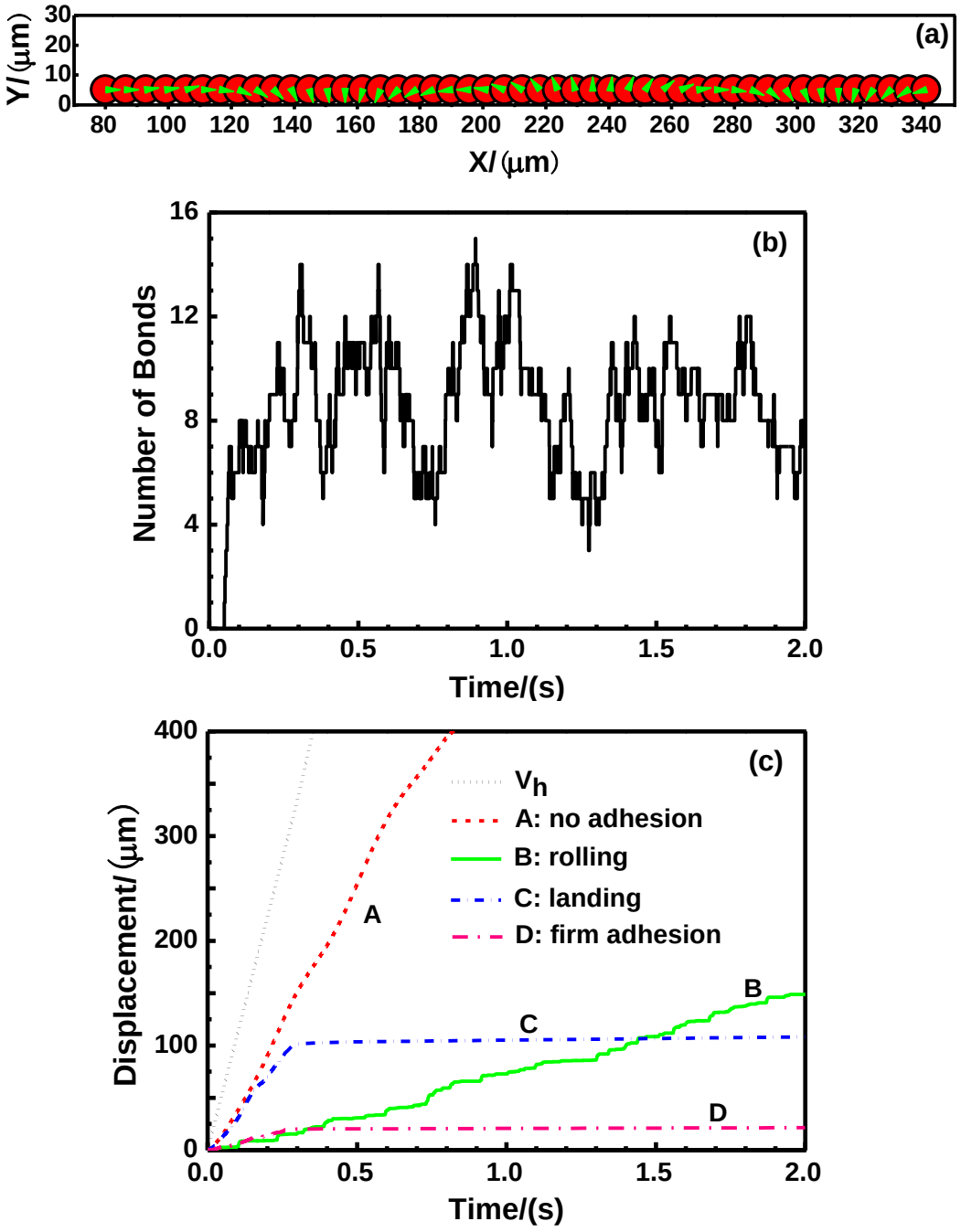

Fig. 4. (a) The trace of the representative rolling leukocyte, (b) The number of bonds of the representative rolling leukocyte, and (c) The representative leukocyte adhesion states: A. no adhesion: γ = 0.5 Å, k_r^0 = 1000 s^{-1}; B. rolling: γ = 0.5 Å, k_r^0 = 200 s^{-1}; C. landing: γ = 0.75 Å, k_r^0 = 20 s^{-1}; D. firm adhesion: γ = 0.5 Å, k_r^0 = 20 s^{-1}

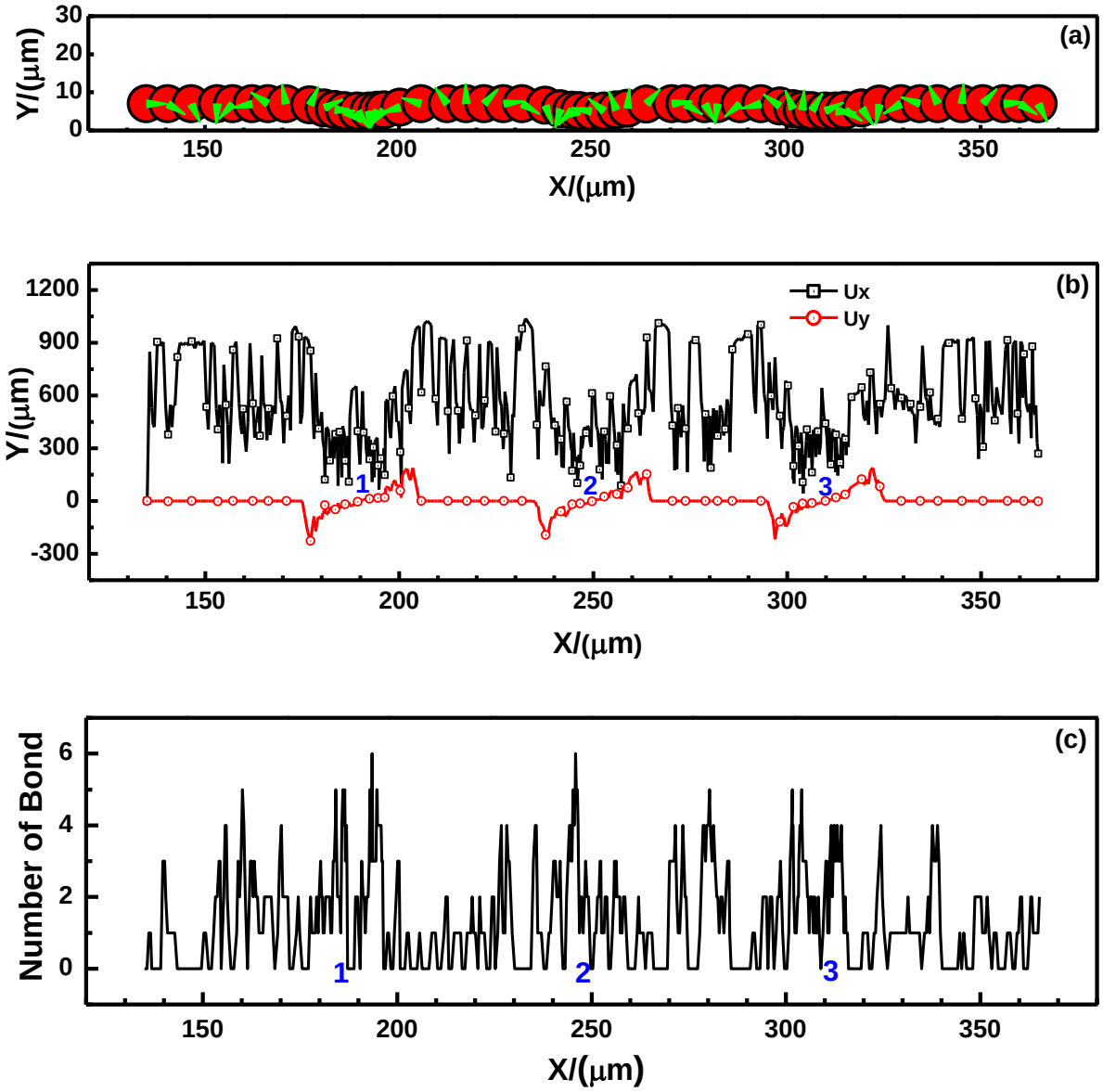

Fig. 5. Referential case: (a) The trace of the translating and rotating cell, (b) The *x*, *y*-component velocities of the cell, and (c) The number of bonds in the uneven micro-vessel.

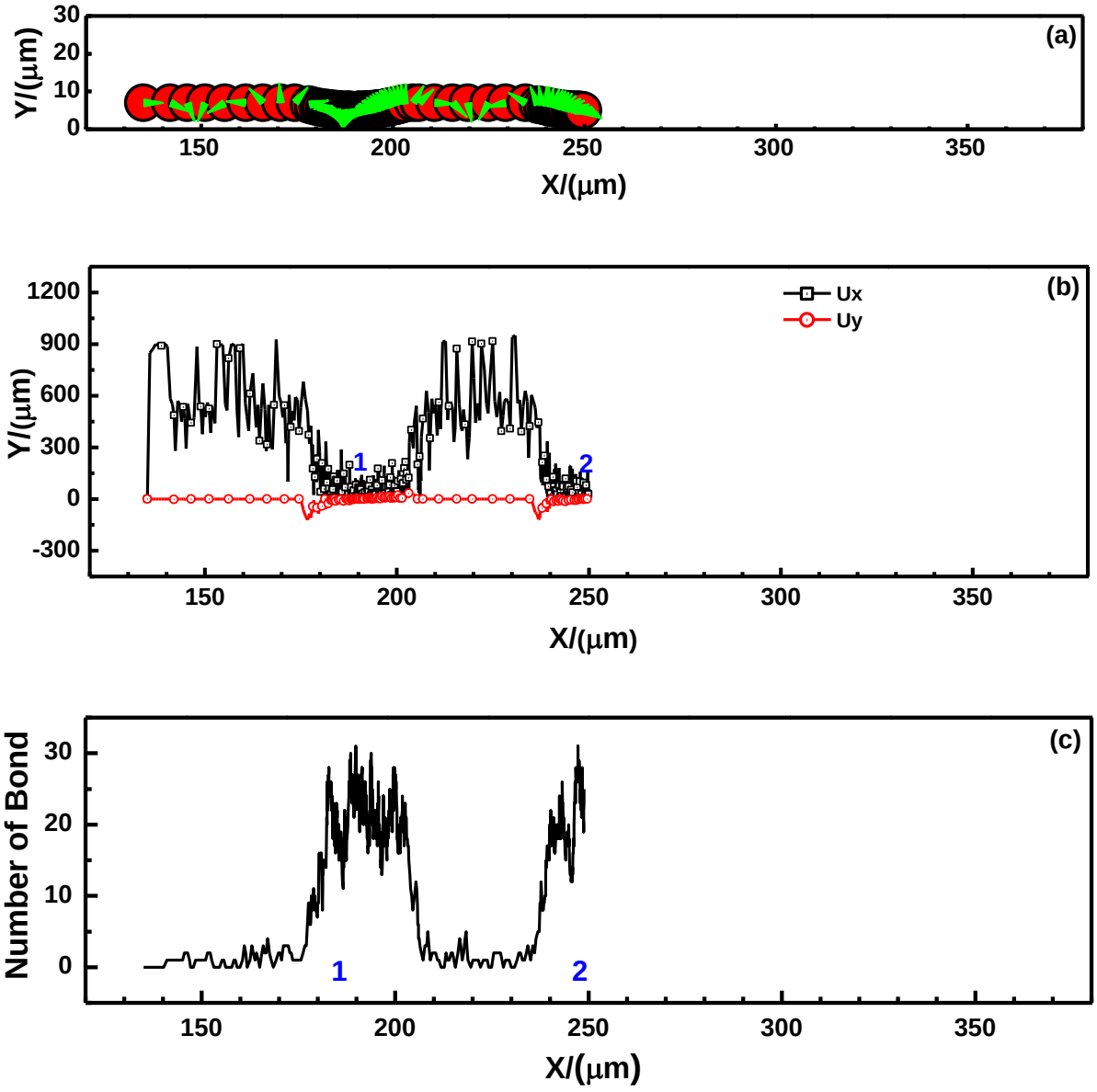

Fig. 6. The effect of ligand density on cell adhesion in the uneven micro-vessel. (a) The trace of the cell, (b) The *x*, *y*-component velocities of the cell, and (c) The number of bonds between cell and ECs.

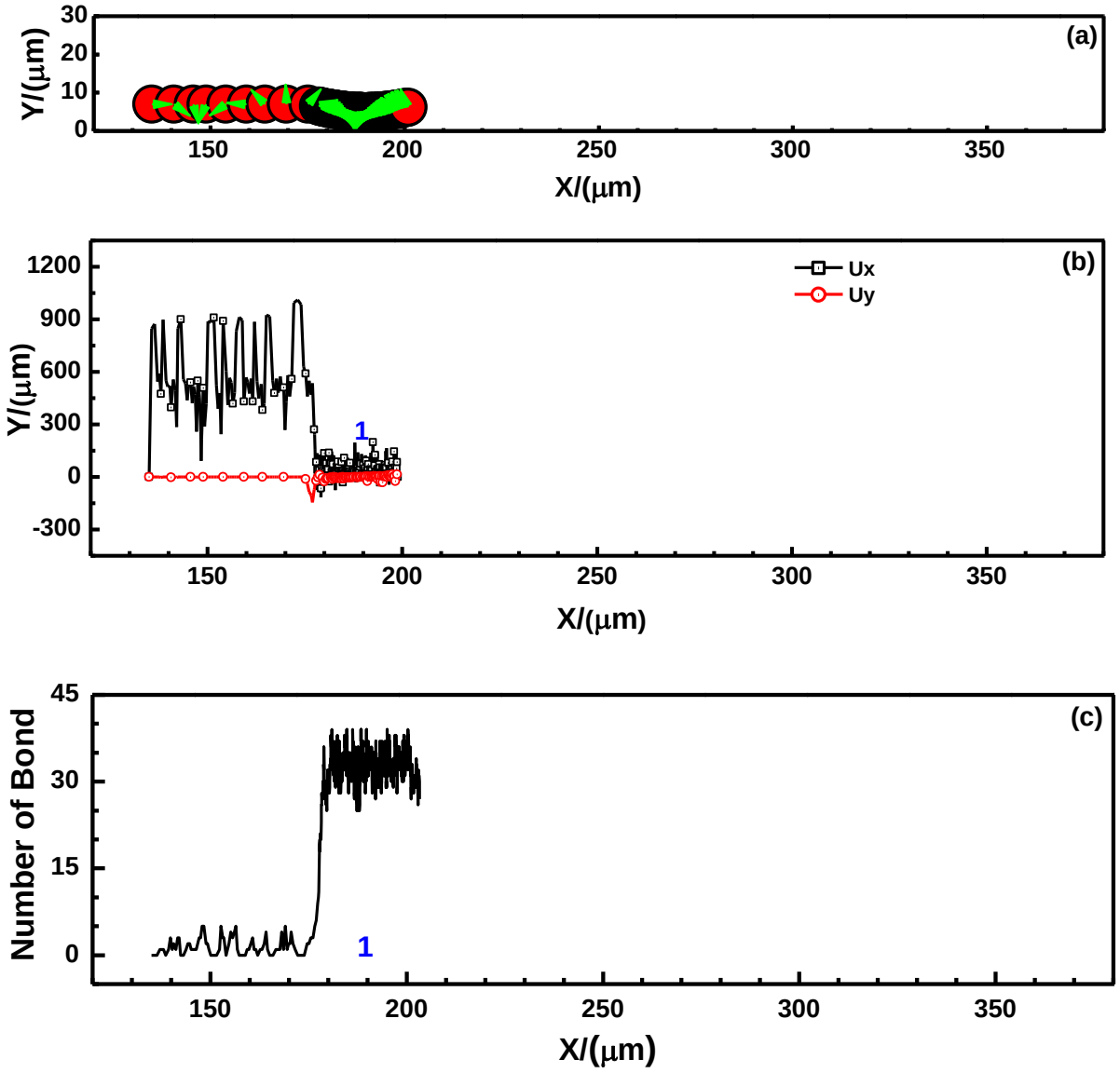

Fig. 7. The effect of forward reaction rate on cell adhesion in the uneven micro-vessel. (a) The trace of the cell, (b) The *x*, *y*-component velocities of the cell, and (c) The number of bonds between cell and ECs.